

# Phase diagram of vortices in the quasi-two-dimensional organic superconductor $\alpha$ -(BEDT-TTF)<sub>2</sub>NH<sub>4</sub>Hg(SCN)<sub>4</sub>: A system of pancake vortices with out-of-plane coupling dominated by the electromagnetic energy

Hiromi Taniguchi and Yasuhiro Nakazawa  
*Institute for Molecular Science, Myodaiji, Okazaki 444, Japan*

Kazushi Kanoda  
*Institute for Molecular Science, Myodaiji, Okazaki 444, Japan*  
*and Department of Applied Physics, University of Tokyo, Hongo, Bunkyo-ku, Tokyo 113, Japan*  
 (Received 29 July 1997)

Anisotropy and field-temperature ( $H$ - $T$ ) phase diagram of the quasi-two-dimensional superconductor,  $\alpha$ -(BEDT-TTF)<sub>2</sub>NH<sub>4</sub>Hg(SCN)<sub>4</sub>, were investigated through the specific heat, ac complex susceptibility  $\chi = \chi' - i\chi''$ , and resistivity measurements under zero field and dc fields normal to the conducting plane. The anisotropy parameter  $\gamma$  was determined to be as large as  $\sim 10^3$ . In the vortex state of this highly anisotropic superconductor, it was found that the onset of the in-plane and out-of-plane ac susceptibility forms a characteristic line well below the  $H_{c2}$  line determined by the specific-heat measurements. The absence of the frequency dependence in the out-of-plane susceptibility suggests that this is a melting line of vortices, rather than a crossover of vortex dynamics. The out-of-plane resistivity measurements show that the interlayer coherence between pancake vortices is established well above the melting line. Considering the anisotropy parameter obtained in the present study, the pancake vortices in this superconductor is viewed as an assembly coupled mainly through the electromagnetic energy in the out-of-plane direction. According to this feature, the two characteristic lines in the  $H$ - $T$  diagram were qualitatively explained by the recent melting and decoupling theories taking account of the electromagnetic coupling. [S0163-1829(98)01302-2]

## I. INTRODUCTION

The vortex state of layered type-II superconductors attracts current interest. It is now a widely accepted concept that the thermal fluctuations of vortices give rise to vortex lattice melting, which was observed in high- $T_c$  oxide superconductors by several measurements.<sup>1-3</sup> The melting phenomenon is considered to result from the unusual values of superconducting parameters, such as a high transition temperature  $T_c$ , a high anisotropy  $\gamma$ , and a large Ginzburg-Landau parameter  $\kappa$ .<sup>4</sup> On the other hand, a short out-of-plane coherence length  $\xi_{\perp}$ , which enhances the out-of-plane discrete nature in the vortices,<sup>5</sup> leads the vortex-line assembly to a system of the pancake vortices in a dc field perpendicular to the conducting plane. This concept of pancake vortices becomes realistic in a highly two-dimensional superconductors of high- $T_c$  oxides especially in Bi<sub>2</sub>Sr<sub>2</sub>CaCu<sub>2</sub>O<sub>8+ $\delta$</sub>  (abbreviated BSCCO hereafter). In such a superconductor, a complicated field-temperature ( $H$ - $T$ ) phase diagram is proposed theoretically<sup>6-8</sup> and suggested experimentally;<sup>9-13</sup> phase boundaries of melting, dimensional crossover, and decoupling appear in between the upper critical field  $H_{c2}$ , and the lower critical field  $H_{c1}$ , in the  $H$ - $T$  plane. In this way, two important ingredients, the thermal fluctuations and the quasi-two-dimensionality of vortices, make the  $H$ - $T$  phase diagram interesting, although they are mutually related. The former is evaluated by the Ginzburg number,<sup>4</sup>  $Gi = \frac{1}{2}(k_B T_c \gamma / H_c(0) \xi_{\parallel}^3)^2$ , and the latter is characterized by the anisotropy parameter,  $\gamma = (m_{\perp} / m_{\parallel})^{1/2}$ , where  $H_c(0)$  is the thermodynamic critical field and  $m_{\perp} (m_{\parallel})$  is the out-of-plane (in-plane) effective mass.

The BEDT-TTF molecule-based organic superconductors are another family of layered superconductors which are prospective for the study of the vortex state in the sense that these systems have large Ginzburg number and high anisotropy, where BEDT-TTF denotes bis(ethylenedithio)tetraathiafulvalene and is abbreviated to ET. For example,  $\kappa$ -(BEDT-TTF)<sub>2</sub>Cu(NCS)<sub>2</sub> (abbreviated ET-NCS), a representative of the 10-K class of organic superconductors, has a strong resemblance<sup>14</sup> to BSCCO in the superconductive parameters, which will be mentioned below. So one can expect that there are similarities in the vortex state between these two materials. In fact, anomalous vortex dynamics and possible melting transition were suggested by NMR studies<sup>15</sup> of this material just prior to the oxides. Moreover, it is emphasized that a large number of ET-based superconductors with layered structure, which are now available, are expected to span a wide range of the superconductive parameters. Roughly speaking, the thickness of the anion layer is a measure of the size of anisotropy. In this sense, the titled compound,  $\alpha$ -(BEDT-TTF)<sub>2</sub>NH<sub>4</sub>Hg(SCN)<sub>4</sub> (abbreviated ET-NH<sub>4</sub> hereafter) is outstanding in that the insulating anion layer is the thickest among the family of ET-based superconductors;<sup>16</sup> the layer period in the out-of-plane direction is about 20 Å for ET-NH<sub>4</sub>, while it is about 15 Å for ET-NCS (15 Å for BSCCO). Therefore, ET-NH<sub>4</sub> is expected to give higher anisotropy in the superconductivity than ET-NCS although the transition temperature  $T_c$  of  $\sim 1$  K is rather low.<sup>17,18</sup>

Previously we characterized the normal and superconducting states by resistive and inductive measurements and found that the anisotropy parameter  $\gamma$  amounts to the order

of  $10^3$  (Ref. 19), which is greater than the values of about 250 in ET-NCS and about 150 in BSCCO. (A comparative discussion on the parameters of these two materials will be given later.) The qualitatively different profiles of in-plane and out-of-plane resistive transitions and the quite long out-of-plane penetration depth of 1.4 mm both indicate a weak interlayer coupling of superconductivity.<sup>19</sup> These features are expected to enhance the two-dimensional character of vortices and possibly to provide a new  $H$ - $T$  phase diagram. Thus we consider that this 1 K organic superconductor serves as an extreme two-dimensional case for comprehensive understanding of statistics and dynamics of the pancake vortices.

In the present work, the phenomenological aspects of the superconductivity in ET-NH<sub>4</sub> was studied in the following two steps. The first step is characterization of anisotropy through the measurement of resistivity in the normal state and penetration depth in the superconducting state at a zero field. Although we have already reported the anisotropy parameter in our previous communication,<sup>19</sup> details of the determination and analysis are given in the present paper. The second step, which is a main part of this paper, is to clarify the vortex state of ET-NH<sub>4</sub>. Under dc fields perpendicular to the conducting plane, we measured ac complex susceptibility  $\chi = \chi' - i\chi''$  and resistivity in both the in-plane and the out-of-plane configurations, as well as specific heat. Through these measurements, two characteristic lines have been found below the  $H_{c2}$  boundary in the  $H$ - $T$  plane. One is a line which suggests the melting of vortices, and the other is a line indicating the rapid growth of out-of-plane coherence between the mobile pancake vortices.

## II. EXPERIMENTAL

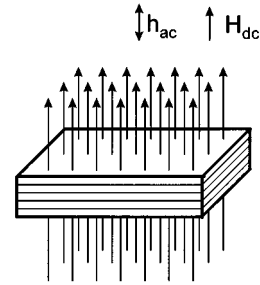
Single crystals used in this study were grown by the electrochemical method.<sup>16</sup> The specific heat, ac susceptibility, and resistivity were measured for single crystals in a zero or several dc fields perpendicular to the conducting plane.

The specific heat was measured for a crystal weighing 5.96 mg in a temperature range of 0.25–1.2 K by the thermal relaxation method. A thin sapphire plate ( $2 \times 2 \times 0.12$  mm<sup>3</sup>) was used as a bolometer on which a calibrated RuO<sub>2</sub> thermometer and a film-manganin heater were attached. The calorimetry unit was mounted in a dilution refrigerator.

The samples with typical dimensions of  $1 \times 0.5 \times 0.1$  mm<sup>3</sup> were used for the resistivity measurements while larger ones with dimensions of  $(3-1) \times 1 \times 0.5$  mm<sup>3</sup> were for the susceptibility measurements. The resistivity and ac susceptibility measurements were performed in a <sup>3</sup>He refrigerator. In the case of the zero-field measurement, the system was surrounded by double  $\mu$ -metal shields to shut out the earth field, which can influence the superconductivity in a low- $T_c$  material such as the present system. The residual dc field was reduced to less than 1 mOe, which was confirmed by a Hall sensor. The measurement platforms including the sample were kept soaked in liquid <sup>3</sup>He, so that the stability and the agreement between temperatures at the thermometer and the sample were achieved. The calibrated Cernox sensors were used as a thermometer. The lowest temperature achievable was 0.41 K.

The ac susceptibility was measured using the standard mutual-inductance technique with two-phase lock-in detec-

(a) Field configuration of compression mode



(b) Field configuration of tilt mode

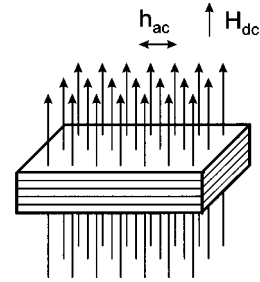


FIG. 1. Field configurations in the ac susceptibility measurements under dc fields. The directions of ac field  $h_{ac}$  and dc field  $H_{dc}$ , in the two configurations are shown.

tion. The apparatus was calibrated by two reference samples of conventional superconductors, Cd ( $T_c = 0.52$  K) and Al ( $T_c = 1.18$  K). While the dc fields were always applied perpendicular to the layers, the ac field was perpendicular or parallel to the layers, as shown in Fig. 1. The former geometry [Fig. 1(a)] gives the susceptibility in the compression mode of the vortices, while the latter [Fig. 1(b)] gives that in the tilt mode. In this paper, the ac susceptibility in the former configuration, where a shielding current flows within the plane, is called in-plane ac susceptibility, while that in the latter configuration, where both the in-plane and the out-of-plane shielding currents flow, is called out-of-plane ac susceptibility because the out-of-plane shielding current determines susceptibility, as will be explained later.

The resistivity measurements were performed in the in-plane and out-of-plane configurations, where the dc current was injected in directions parallel and perpendicular to the plane, respectively. The gold wires of 15  $\mu$ m in diameter were attached to single crystals with carbon paste. The resistance of each contact was less than 10  $\Omega$  at 0.5 K.

## III. CHARACTERIZATION OF ANISOTROPY PARAMETER AND UPPER CRITICAL FIELD

### A. Anisotropy of resistivity

The ET-NH<sub>4</sub> is a highly anisotropic conductor of thick plates. For such a kind of crystal, the absolute value of in-plane resistivity,  $\rho_{\parallel}$ , is not easy to determine with reliable accuracy because of difficulty of making up a homogeneous current distribution, while that of out-of-plane resistivity  $\rho_{\perp}$

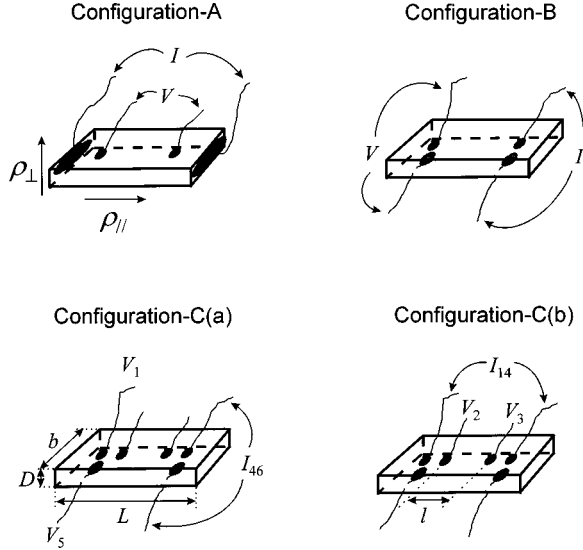


FIG. 2. Configurations of leads in the present resistivity measurements. Directions of in-plane resistivity  $\rho_{\parallel}$  and out-of-plane resistivity  $\rho_{\perp}$  are also shown.

can be obtained by the standard four-terminal method with the use of the benefit that the high two-dimensionality tends to permit the flow of the homogeneous current in the out-of-plane direction. Figure 2 shows the configurations of leads adopted in the present study. In the first method to evaluate the anisotropy of resistivity, the in-plane (current  $\parallel$  conducting layers) and out-of-plane (current  $\perp$  conducting layers) resistivity measurements were independently made for 5 and 25 crystals with configuration-A and configuration-B, respectively. (This method is named method 1.) Most samples show metallic temperature variation in resistivity in both directions in a whole temperature range below 300 K. The absolute values of  $\rho_{\parallel}$  and  $\rho_{\perp}$  are 2–7 m $\Omega$  cm and 2–3 k $\Omega$  cm at room temperature and decrease to  $10^{-2}$ – $10^{-1}$  m $\Omega$  cm and 20–40  $\Omega$  cm at 3 K, respectively. The anisotropy ratio of the in-plane and out-of-plane values is in a range of  $10^5$ – $10^6$  from room temperature to 3 K. The averaged values over the measured samples are  $7.2 \times 10^5$  (285 K) and  $7.9 \times 10^5$  (3 K). These are listed in Table I with the averaged values of  $RRR_{\parallel}$  and  $RRR_{\perp}$ , where  $RRR$  denotes the residual resistivity ratio,  $\rho(285 \text{ K})/\rho(3 \text{ K})$ .

In the second method (method 2) to evaluate  $\rho_{\perp}/\rho_{\parallel}$ , a crystal which has the most symmetrical and nearly rectangular shape was chosen among the crystals grown. The  $\rho_{\parallel}$  and  $\rho_{\perp}$  were examined for this identical crystal by the six-terminal method with four leads on the top surface and two leads on the bottom surface of the crystal [configurations-C(a) and (b) in Fig. 2]. The results were analyzed with the method which is based on the determination of the inhomogeneous

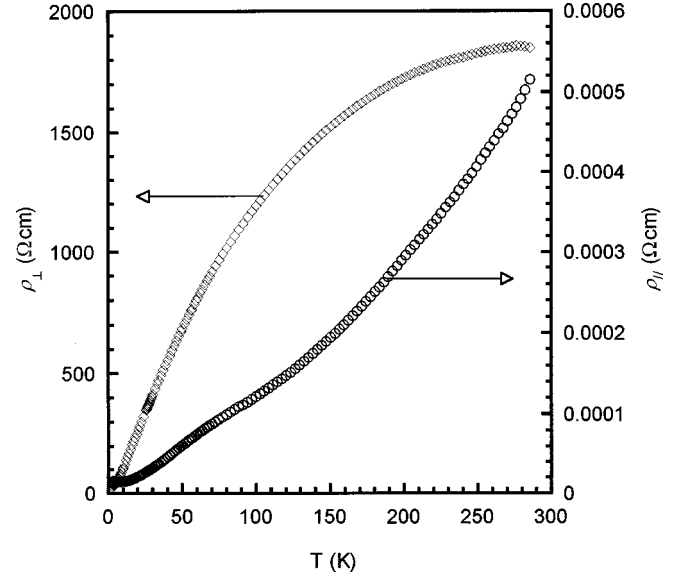


FIG. 3. The temperature dependence of  $\rho_{\parallel}$  and  $\rho_{\perp}$ .

current distribution in a crystal by solving the Laplace equation. A similar method was applied to a single crystal of BSCCO by Bush *et al.*<sup>20</sup> In configuration-C(a), the absolute value of  $\rho_{\perp}$  was obtained by multiplying  $R_{\perp}$  by  $(L \times b)/D$  as in method 1, where  $R_{\perp} = (V_1 - V_5)/I_{46}$ , and  $L$ ,  $b$ , and  $D$  are dimensions of the crystal. Next, the current-voltage configuration was changed to Configuration-C(b), which gave the surface in-plane resistivity,  $R_{\parallel}^s = (V_2 - V_3)/I_{14}$ . In a two-dimensional bulk material, the absolute value of  $\rho_{\parallel}$  is approximately given through a relation of  $(\rho_{\parallel}\rho_{\perp})^{1/2} \sim (R_{\parallel}^s \times b)/2 \sin[\pi l/2L]$  with the value of  $\rho_{\perp}$ , where  $l$  is a distance between the voltage electrodes [for details, see Ref. 20]. In this way, both  $\rho_{\parallel}$  and  $\rho_{\perp}$  are simultaneously obtained for an identical crystal and are shown as a function of temperature in Fig. 3. While  $\rho_{\parallel}$  shows a positive curvature,  $\rho_{\perp}$  does a moderate negative curvature. These behaviors well reproduce the results obtained in method 1. It is well known that resistivity of BSCCO (Ref. 21) is semiconducting in the out-of-plane direction, while metallic in the in-plane one, and that ET-NCS (Ref. 22) is metallic at low temperatures, while semiconducting at higher temperatures in both directions. In contrast to these materials, ET-NH<sub>4</sub> has nothing anomalous in the resistivity in spite of the extreme two-dimensional nature. The application of method 2 to the present sample yielded the values of  $\rho_{\parallel} = 0.51 \text{ m}\Omega \text{ cm}$  and  $\rho_{\perp} = 1800 \text{ }\Omega \text{ cm}$  at 285 K and  $\rho_{\parallel} = 0.015 \text{ m}\Omega \text{ cm}$  and  $\rho_{\perp} = 26 \text{ }\Omega \text{ cm}$  at 3 K. The anisotropy of resistivity,  $\rho_{\perp}/\rho_{\parallel}$ , is  $3.6 \times 10^6$  at 285 K and  $1.7 \times 10^6$  at 3 K, which are also listed in Table I with  $RRR$ 's in both directions.

As seen in Table I, there is no serious difference in the residual resistivity ratio,  $RRR_{\parallel}$  and  $RRR_{\perp}$ , between the two methods. As for the anisotropy parameter, there is a factorial difference; the anisotropy of resistivity at 3 K is  $7.9 \times 10^5$  and  $1.7 \times 10^6$  in methods 1 and 2, respectively. The difference is not only attributable to the sample dependence but also to the methodological ambiguity coming from the difficulty of the determination of the absolute value of resistivity in such a highly anisotropic conductor. In any case,  $\rho_{\perp}/\rho_{\parallel}$ ,

TABLE I. Anisotropy of resistivity at 3 and 285 K, determined by the two methods described in the text. The residual resistivity ratio (RRR) is also listed.

Method	$\rho_{\perp}/\rho_{\parallel}$ at 285 K	$\rho_{\perp}/\rho_{\parallel}$ at 3 K	$RRR_{\parallel}$	$RRR_{\perp}$
Method 1	$7.2 \times 10^5$	$7.9 \times 10^5$	71	64
Method 2	$3.6 \times 10^6$	$1.7 \times 10^6$	34	70

one of the important material parameters, is concluded to be  $\sim 10^6$ , which is used in the following discussion.

### B. Anisotropy of penetration depth

In this section, anisotropy of penetration depth  $\lambda_{\perp}/\lambda_{\parallel}$  is discussed. While  $\rho_{\perp}/\rho_{\parallel}$  reflects the normal-state anisotropy,  $\lambda_{\perp}/\lambda_{\parallel}$  is a measure of the anisotropy of superconductivity. First, an inference of the value of  $\lambda_{\parallel}$ , which could not be determined in the present experiments, is surveyed below. The in-plane penetration depth  $\lambda_{\parallel}$  is estimated by the London formula of  $\lambda_{\parallel} = \sqrt{m^*c^2/(4\pi ne^2)}$ , which is determined by the effective electron mass  $m^*$  and density  $n$ . The applicability of the London theory is examined in the case of ET-NCS, where experimental values of  $\lambda_{\parallel}$  are available; the  $\mu$ SR (Ref. 23) and magnetization<sup>24</sup> measurements yielded values in a range of 0.65–1.0  $\mu\text{m}$ , which is represented by an averaged value of 0.8  $\mu\text{m}$ . If we adopt the cyclotron mass deduced by the Shubnikov–de Haas (SdH) oscillations as the effective mass,  $m^*$ , the values of  $m^* = 6.9m_0$  (Ref. 25) and  $n = 1.2 \times 10^{21} \text{ cm}^{-3}$  give a value of  $\lambda_{\parallel} = 0.40 \mu\text{m}$ , which is appreciably different from the experimental value. There may be several reasons for this discrepancy. For example, the London theory assumes a homogeneous electron medium of a carrier density  $n$ , while in reality the carrier density has an inhomogeneous distribution due to the layered structure in ET-NCS. For this reason, direct application of the London formula does not seem plausible. Then, we consider that the modification of the experimental value of  $\lambda_{\parallel}$  of ET-NCS by multiplying a factor of  $(m_{\text{NH}_4}^*/m_{\text{NCS}}^*)^{1/2}(n_{\text{NCS}}/n_{\text{NH}_4})^{1/2}$  is one of the realistic methods to give  $\lambda_{\parallel}$  of ET-NH<sub>4</sub>, since the two salts have a similar kind of Fermi-surface topology; an originally large cylindrical Fermi surface which has the same cross-sectional area as the Brillouin zone ( $S_{\text{BZ}}$ ) crosses the zone boundary, resulting in one closed Fermi surface and a pair of open Fermi surfaces. While the value of  $m_{\text{NCS}}^*$  is obtained as  $6.9m_0$  from the magnetic breakdown oscillation where the cyclotron trajectory covers the whole Fermi surfaces (so-called  $\beta$  orbit) at high fields, there was no observed breakdown in ET-NH<sub>4</sub> even at the high fields achievable. Then, we estimated the ratio,  $m_{\text{NH}_4}^*/m_{\text{NCS}}^*$ , from the cyclotron mass of the closed Fermi surface (so-called  $\alpha$  orbit) in the two salts since the both show clear  $\alpha$ -orbit SdH oscillations with similar cross-sectional areas (13 and 15 % of  $S_{\text{BZ}}$  for ET-NH<sub>4</sub> and ET-NCS, respectively). Using  $m_{\text{NH}_4}^*(\alpha \text{ orbit}) = 2.4m_0$  (Ref. 26),  $m_{\text{NCS}}^*(\alpha \text{ orbit}) = 3.5m_0$  (Refs. 25, 27),  $n_{\text{NH}_4} = 1.00 \times 10^{21} \text{ (cm}^{-3}\text{)}$  and  $n_{\text{NCS}} = 1.22 \times 10^{21} \text{ (cm}^{-3}\text{)}$ ,  $\lambda_{\parallel}$  of ET-NH<sub>4</sub> is estimated at 0.7  $\mu\text{m}$ .

On the other hand, the out-of-plane penetration depth  $\lambda_{\perp}$  could be determined by the out-of-plane ac susceptibility measurement under a zero dc field and with an ac field applied parallel to the plane. Since this was reported in our paper,<sup>19</sup> the experimental procedure is not mentioned in detail here. In the quasi-two-dimensional superconductor, the out-of-plane penetration depth is regarded as the Josephson penetration depth which depends on the Josephson critical current.<sup>28</sup> If the out-of-plane coupling is weak,  $\lambda_{\perp}$  amounts to a large value, reflecting small Josephson critical current. Since the superconducting coupling between the layers in ET-NH<sub>4</sub> must be weak due to thick insulating anion layers,

the length scale of  $\lambda_{\perp}$  is expected to be detectable even through the macroscopic probe. Indeed, the ac susceptibility showed a considerable decrease from the perfect diamagnetism in the parallel field geometry, indicating that the value of  $\lambda_{\perp}$  is comparable to the crystal size. The value of  $\lambda_{\perp}$  was directly calculated from the out-of-plane ac susceptibility, using the relation

$$-4\pi\chi' = 1 - (2\lambda_{\perp}/L)\tanh(L/2\lambda_{\perp}), \quad (1)$$

where  $L$  is the sample length along the plane and perpendicular to the ac field. This formula with the values of  $L$  and  $\chi'$  gave a value of  $\lambda_{\perp} = 1.4 \text{ mm}$  at 0 K. Reproducibility of this result was confirmed in the measurements of five crystals with different dimension  $L$  (For details, see Ref. 19). This macroscopic value demonstrates the Josephson nature of the out-of-plane coupling.

The in-plane and out-of-plane penetration depths of  $\lambda_{\parallel} = 0.7 \mu\text{m}$  and  $\lambda_{\perp} = 1.4 \text{ mm}$  give an anisotropy parameter,  $\gamma = \lambda_{\perp}/\lambda_{\parallel} = (m_{\perp}/m_{\parallel})^{1/2}$ , as 2000. As discussed in the previous section, the anisotropy of resistivity is in a range of  $\sim 10^6$ , which is fairly consistent with this value. The relation of  $\lambda_{\perp}/\lambda_{\parallel} = (\rho_{\perp}/\rho_{\parallel})^{1/2}$  is roughly fulfilled.

### C. Upper critical field; determination by specific-heat measurements under dc fields normal to the conducting plane

In this section, we determine upper critical field  $H_{c2}$  and coherence length  $\xi$  of ET-NH<sub>4</sub>. In a superconductor which has large fluctuations, resistivity is not a useful probe for a definition of  $H_{c2}(T)$ , because the superconducting fluctuations in a higher temperature side and the fluctuations of vortices (flux flow) in the lower temperature side make the resistive  $H_{c2}(T)$  line ambiguous. It is also believed that other physical quantities in such a system does not show so clear transition at  $H_{c2}(T)$  under fields as in the conventional superconductors. One of the reasonable definitions of the mean-field-like  $H_{c2}(T)$  is by the thermodynamic quantity. Indeed, it was shown even in a low- $T_c$  superconductor such as  $\text{Ti}_2\text{Ba}_2\text{CuO}_{6+\delta}$  ( $T_c \sim 15 \text{ K}$ ) that  $H_{c2}(T)$  determined by the specific-heat measurements have a quite different temperature dependence from that determined by resistivity.<sup>29</sup> This indicates that the effect of fluctuations can destroy the mean-field-like resistive transition even in the low- $T_c$  superconductors. So we adopted the specific heat as a measure of  $H_{c2}(T)$ .

Figure 4 shows the superconducting components of the electronic specific heat  $C_p/T$  in several magnetic fields, defined as the difference between specific heats in the superconducting and normal states, i.e.,  $C_p = C(H) - C(H = 8 \text{ T})$ . It is noted that the system is in the normal state in a field of 8 T. Assuming the mean-field transition curve predicted by BCS theory as shown by the solid line, the transition temperature  $T_c(H)$  was determined in each field so that the BCS curve compensates the entropy of the observed curve from the thermodynamic point of view. Thus, a  $H_{c2}(T)$  line was defined by a set of  $T_c(H)$  data as a characteristic boundary of occurrence of superconductivity. Figure 5 shows the results on the present two crystals. Temperature derivative of upper critical fields near  $T_c$  was obtained as  $[dH_{c2}(T)/dT]_{T_c} = 0.08 \text{ T/K}$  from the present data; this value

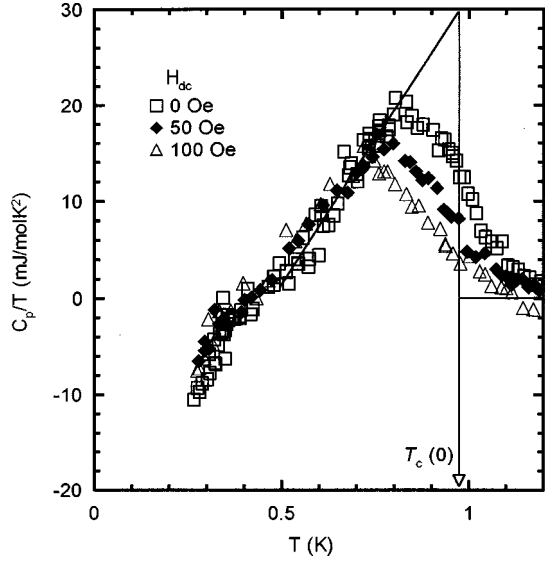


FIG. 4. The temperature and field dependence of the superconducting component of electronic specific heat;  $C_p/T$  vs  $T$  plot, where  $C_p = C(H) - C(H = 8 \text{ T})$ . The transition temperatures in each field are named  $T_c(H)$ . Representatively, the zero-field case  $T_c(0)$  is shown.

is slightly different from  $[-dH_{c2}(T)/dT]_{T_c} = 0.1 \pm 0.02 \text{ T/K}$  determined by Andracka *et al.*<sup>30</sup> who defined  $T_c(H)$  as the temperature giving the maximum in  $C/T$ . Using the present value and the Ginzburg-Landau (GL) theory, the GL coherence length  $\xi_{\parallel}$  is estimated at about  $500 \text{ \AA}$ .

#### IV. SUPERCONDUCTING PARAMETERS; COMPARISON WITH OTHER QUASI-TWO-DIMENSIONAL SUPERCONDUCTORS

The superconducting parameters deduced from the experiment and inference in the previous sections are all listed in

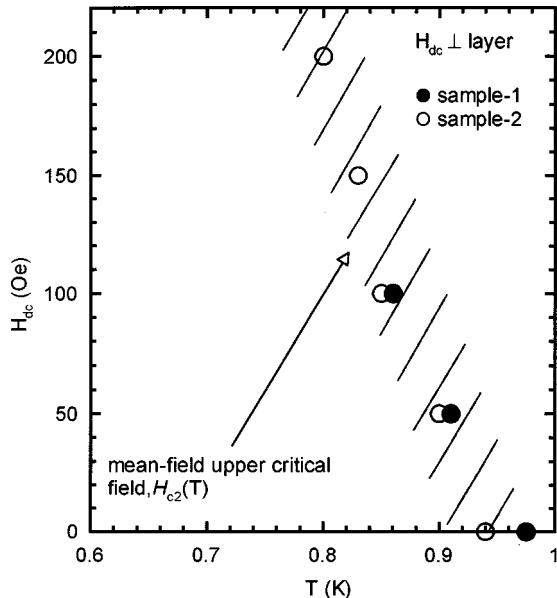


FIG. 5. Thermodynamic transition temperatures  $T_c(H)$  determined by the specific-heat measurements under fields for two crystals, which form the mean-field  $H_{c2}$  line in the  $H$ - $T$  plane.

Table II with those of two other quasi-two-dimensional superconductors, ET-NCS [ $\kappa$ -(BEDT-TTF) $_2$ Cu(NCS) $_2$ ] (Ref. 31) and BSCCO ( $\text{Bi}_2\text{Sr}_2\text{CaCu}_2\text{O}_{8+\delta}$ ).<sup>32</sup> These parameters must dominate the character of the vortex state, so that knowledge of them is quite informative to argue the  $H$ - $T$  phase diagram with the experimental results. Using the above parameters, the Ginzburg number,  $Gi$ , of ET-NH $_4$  is estimated at 0.1, which is considerably larger than those of the conventional materials, e.g.,  $5 \times 10^{-7}$  for Nb, and also larger than that of  $\text{YBa}_2\text{Cu}_3\text{O}_{7-\delta}$  (0.01). Because  $Gi$  measures the size of vortex fluctuations, a larger value is expected to give a wider range of the vortex-liquid phase in the  $H$ - $T$  plane.

Another feature distinctive from other materials is the large in-plane GL coherence length  $\xi_{\parallel}$ , which is one order of magnitude larger than those of the other two superconductors. This is partly because of the low transition temperature. As for the parameters related to anisotropy or strength of out-of-plane coupling, the anisotropy parameter  $\gamma$ , and concomitantly the out-of-plane penetration depth  $\lambda_{\perp}$  are even larger than those of ET-NCS and BSCCO, which belong to a class of highly anisotropic superconductors. One of the reasons giving the extremely high  $\gamma$  is the layer spacing ( $s = 20 \text{ \AA}$ ) larger than those of the others ( $s = 15 \text{ \AA}$ ).

These peculiar characteristics make the vortices in ET-NH $_4$  distinctive; Josephson length  $\gamma s$  is larger than in-plane penetration depth  $\lambda_{\parallel}$ . The relation of  $\gamma s > \lambda_{\parallel}$  means that this superconductor is classified as an extremely anisotropic class of superconductor, while  $\gamma s \leq \lambda_{\parallel}$  in BSCCO and ET-NCS. (The  $\lambda_{\parallel}$  depends on temperature and diverges near  $T_c$ . However, the difference by one order of magnitude between  $\gamma s$  and the 0-K value of  $\lambda_{\parallel}$  means that the relation of  $\gamma s > \lambda_{\parallel}$  holds in a wide temperature range except the vicinity of  $T_c$  in ET-NH $_4$ .) In a quasi-two-dimensional system, the tilt modulus of vortices  $C_{44}$  is determined by the Josephson contribution and the electromagnetic one,<sup>6</sup> of which the typical line-energy scales are  $(\Phi/\gamma s)^2$  and  $(\Phi/\lambda_{\parallel})^2$ , respectively. In this sense, the pancake vortices in ET-NH $_4$  are mainly coupled through the electromagnetic energy in the out-of-plane direction, while those in ET-NCS and BSCCO are coupled by the Josephson energy with a secondary contribution from the electromagnetic energy. This feature distinguishes the present system from the other systems and, therefore, may affect the vortex state, giving a possible variation in the  $H$ - $T$  phase diagram.

#### V. CHARACTERIZATION OF VORTEX STATE

##### A. ac susceptibility

In order to investigate the dynamical response of the vortex systems, the complex ac susceptibility  $\chi = \chi' - i\chi''$  was measured under dc fields in a temperature range of 0.4–1.5 K. The ac field was applied perpendicular [Fig. 1(a)] or parallel [Fig. 1(b)] to the conducting layers. The former configuration gives in-plane susceptibility because a shielding current flows within the planes in the sample, while the latter gives out-of-plane susceptibility because the out-of-plane shielding current dominates the susceptibility due to the large out-of-plane penetration depth. In the in-plane configuration in the vortex state [Fig. 1(a)], the ac field perpendicu-

TABLE II. Superconducting parameters of ET-NH<sub>4</sub>, ET-NCS, and BSCCO. Transition temperature  $T_c$ , in-plane coherence length  $\xi_{\parallel}$ , in-plane and out-of-plane penetration depths  $\lambda_{\parallel}$  and  $\lambda_{\perp}$ , anisotropy parameter  $\gamma$ , interlayer spacing  $s$ , and Josephson length  $\gamma s$ , are listed for the three quasi-two-dimensional superconductors. As for ET-NCS and BSCCO, the parameters were referred from Refs. 31 and 32, respectively.

Parameter	$\alpha$ -(ET) <sub>2</sub> NH <sub>4</sub> Hg(SCN) <sub>4</sub>	$\kappa$ -(ET) <sub>2</sub> Cu(NCS) <sub>2</sub>	Bi <sub>2</sub> Sr <sub>2</sub> CaCu <sub>2</sub> O <sub>8+<math>\delta</math></sub>
$T_c$ (K)	0.95	9.5	91
$\xi_{\parallel}$ (Å)	500	60	30
$\lambda_{\parallel}$ (μm)	0.7	0.8	0.26
$\lambda_{\perp}$ (μm)	1400	200	40
$\gamma$	2000	250	150
$s$ (Å)	20	15	15
$\gamma s$ (μm)	4	0.4	0.2

lar to the plane causes the vortex motion in the compression mode, while in the out-of-plane configuration [Fig. 1(b)] the ac field parallel to the plane acts on the tilt mode. The measurements in these two configurations lead us to understand the mobility of vortices in the two modes.

The in-plane ac susceptibility was measured with an ac field of 0.17 Oe in amplitude under zero and several dc fields. From amplitude dependence of susceptibility, 0.17 Oe is confirmed to be in a region where the susceptibility is independent of amplitude. The frequency of the ac field is 17, 47, 307, and 1007 Hz. Figure 6 shows in-plane susceptibility at 1007 Hz. The transition curve shifts to the lower temperature side in a higher dc field without losing its sharpness. The  $\chi'$  and  $\chi''$  show an appreciable frequency dependence in finite dc fields. A case under a dc field of 55 Oe is shown in Fig. 7; the transition shifts to a lower temperature at a lower frequency. This will be discussed below. There was no observed frequency dependence at a zero field.

The out-of-plane ac susceptibility with an applied ac field of 0.17 Oe in amplitude and 1007 Hz in frequency is shown in Fig. 8. The transition curves in  $\chi'$  do not saturate and the

absolute value reaches only 15% of the full Meissner value at 0.5 K in a zero field. This behavior is attributed to the large out-of-plane penetration depth, as discussed above and in our previous communication.<sup>19</sup> The transition curves shift to the lower temperature side in higher dc fields as in the in-plane configuration. The out-of-plane susceptibility shows no frequency dependence even in finite dc fields in a range of 157–3007 Hz measured in this study. The cases under dc fields of 9 and 36 Oe are shown in Figs. 9(a) and 9(b).

The qualitative difference of the frequency dependence between the two configurations is considered to come from the different ways of stimulating the motion of the vortices. In the in-plane configuration, the ac field initiates activation of the compression mode of the vortex motion. In this situation, the modulation of the vortex density is transmitted from the crystal peripherals toward the center of the sample through the diffusion and/or relaxation process. Thus the characteristic frequency of the response of the whole vortex system to the ac field in this configuration is determined by the ratio of the sample size and the diffusion or relaxation constant and might give an applied-frequency dependence in the susceptibility profile as a crossover behavior.

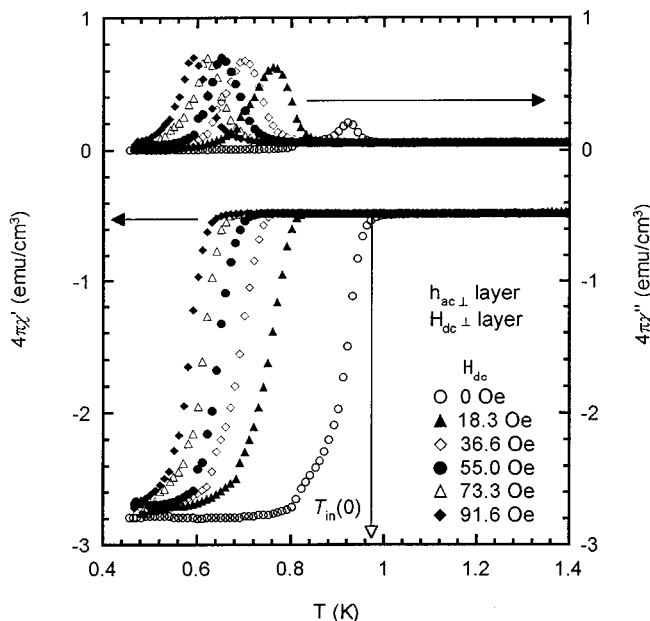


FIG. 6. In-plane ac susceptibility in several dc fields.  $T_{in}(H)$  is the onset temperature of the transition curve;  $T_{in}(0)$  is shown as the zero-field case.

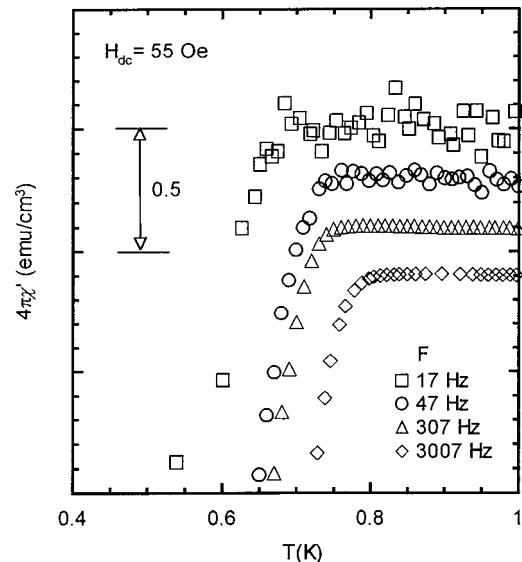


FIG. 7. Frequency dependence of the transition curves of the in-plane ac susceptibility. Origin of the vertical axis is shifted for each frequency for clarity.

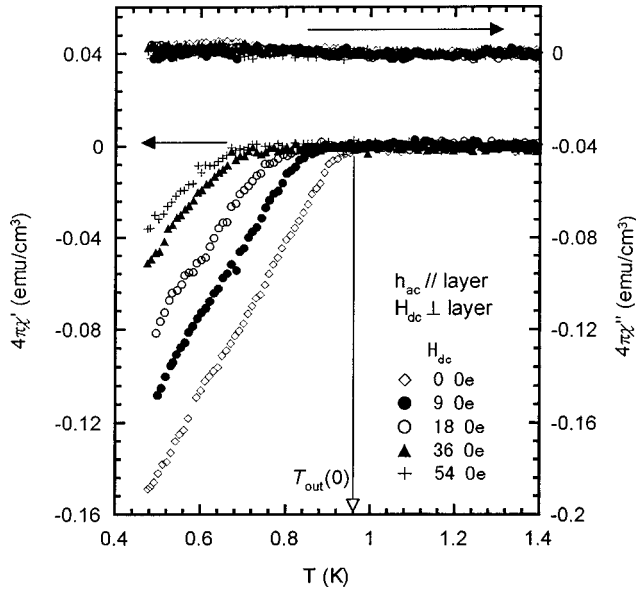


FIG. 8. Out-of-plane ac susceptibility in several dc fields.  $T_{\text{out}}(0)$  is the onset of the out-of-plane inductive transition in a zero field.

On the other hand, application of an ac field parallel to the layer in the vortex state causes the tilting vortex motion in a region of the out-of-plane penetration depth,  $\lambda_{\perp}(0) = 1.4$  mm, which is comparable to or larger than the sample

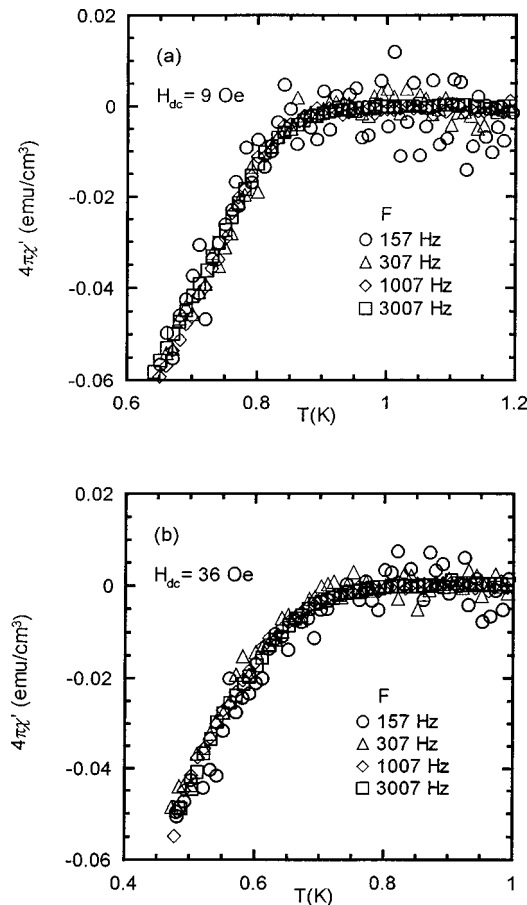


FIG. 9. Frequency dependence of the transition curves of the out-of-plane ac susceptibility under dc fields of 9 Oe (a) and 36 Oe (b).

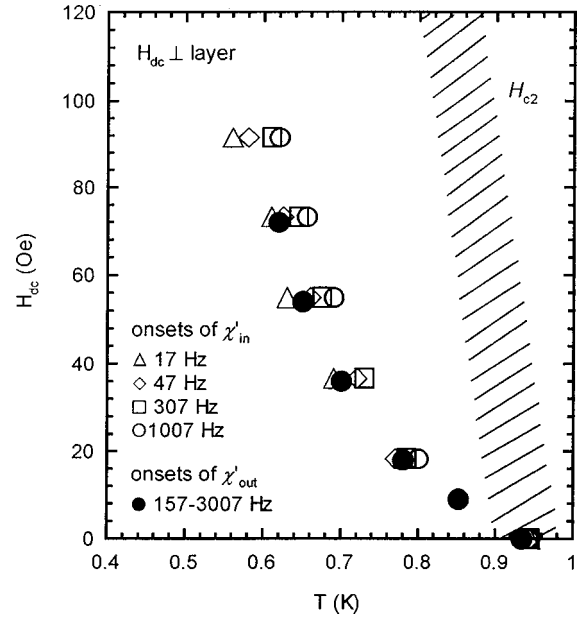


FIG. 10. Onset temperatures of the inductive transitions plotted along with the mean-field  $H_{c2}$  line. The closed circles are the onsets of the out-of-plane ac susceptibility, which show no frequency dependence in the measured range of 157–3007 Hz. The open symbols are the onsets of the in-plane ac susceptibility for 17, 47, 307, and 1007 Hz.

size. This feature permits the whole vortices to be driven directly by the parallel ac field, not via the diffusion or relaxation process. Such a situation is realized only for the present system due to the exceptionally long penetration depth. In this case, the characteristic frequency of the system response is that of the dynamics of the individual vortices, not of the collective mode. The observation of the absence of frequency dependence of the out-of-plane  $\chi'$  in a range of 157–3007 Hz indicates that the dynamics of the individual vortex is much slower than this frequency range below the  $\chi'$  onset temperature and is much faster than that above the onset without a gradual crossover of the characteristic frequency of the vortex dynamics, suggesting a phase transition rather than a crossover. Thus, the frequency dependence appearing only in the in-plane configuration is attributed to the diffusion process of the mobile vortices within the layers. We defined the onset of the inductive transition in the in-plane and out-of-plane  $\chi'(T)$  as functions of measured frequency and applied dc fields. The definitions of them were shown in Figs. 6 and 8, where the onset temperatures were represented as  $T_{\text{in}}(H)$  and  $T_{\text{out}}(H)$ , respectively. They are plotted along with the  $H_{c2}$  line determined by the specific-heat measurement in Fig. 10. The coincidence of the frequency-independent out-of-plane onsets and the low-frequency limit of the in-plane onsets corroborates this interpretation.

Therefore, the drastic change of the vortex mobility at  $T_{\text{out}}(H)$  is likely the phase transition rather than the crossover, and is suggested to be a melting of vortex lattice or glass. The frequency dependence of the collective dynamics in a sub-kHz range implies the viscous nature of the liquid phase near the melting boundary.

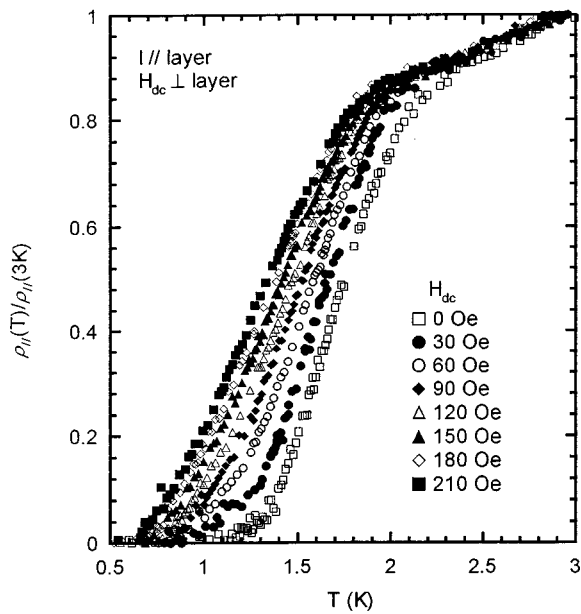


FIG. 11. In-plane resistivity normalized to the value at 3 K under several dc fields applied with a step of 30 Oe from 0 to 210 Oe.

### B. Resistivity

The resistivity measurements were performed in both the in-plane and out-of-plane configurations (configuration C in Fig. 2) under perpendicular dc fields, where the dc current was injected in directions parallel and perpendicular to the conducting layers, respectively. In both of the two configurations, the injected dc currents were 10  $\mu$ A. Figures 11 and 12 show in-plane and out-of-plane resistivities under several dc fields, respectively. The in-plane resistivity  $\rho_{||}$  is normalized to the value of 3 K, while the absolute value of the out-of-plane resistivity  $\rho_{\perp}$  is obtained.

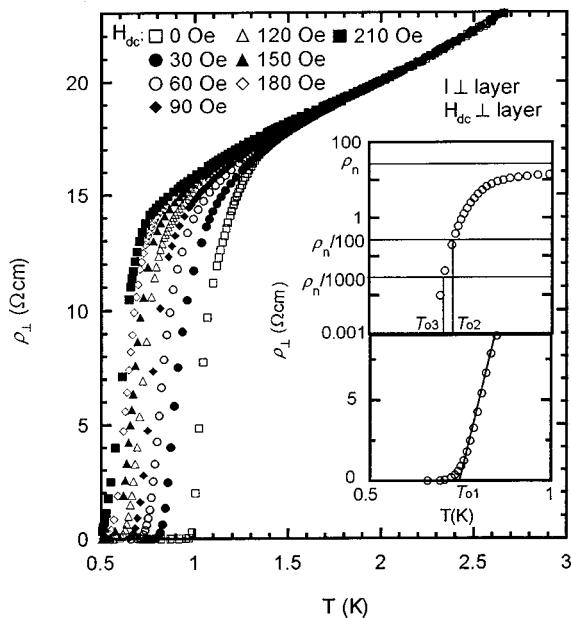


FIG. 12. Out-of-plane resistivity in several dc fields applied with a step of 30 Oe from 0 to 210 Oe.

The profiles of the resistive transitions were qualitatively different between the in-plane and out-of-plane measurements under dc fields as well as a zero field. Even at zero field, the in-plane resistivity shows a gradual transition; the  $\rho_{||}$  starts to decrease around 2.4 K with a tail of positive curvature and vanishes around 1 K. This peculiar behavior was discussed in a previous communication.<sup>19</sup> With the observation of the nonlinearity of the  $I$ - $V$  characteristics reminiscent of the Kosteritz-Thouless transition, we concluded that it was associated with the high two-dimensionality of the present material. Application of dc fields makes the transition curves appreciably broadened. On the other hand, the out-of-plane resistivity exhibits a comparatively sharp transition around 1 K with negative curvature. When the dc field is increased, the transition curve shifts to the lower temperature side. In contrast to the in-plane case, the sharpness of the curvature is scarcely lost even by application of dc fields. This behavior does not seem to be shared by other quasi-two-dimensional superconductors. In BSCCO, the larger the field applied, the broader the transition is. It is reported that resistivity follows an activation type in both directions and that the activation energies are almost the same.<sup>33</sup> In this literature, the behavior was considered to indicate the dynamics of unconnected pancake vortices, which will explain the independence of the activation energy on the current direction.

In the present superconductor, the normal-state in-plane resistivity just above  $T_c$  is quite small compared with other BEDT-TTF salts. Reflecting a large  $Gi$  value, a comparatively low-field range should be of interest. Because the flux-flow resistivity is proportional to the normal-state resistivity and the applied field in the Bardeen-Stephen context for example, the pursuit of the vanishing process of in-plane resistivity in the vortex state in question requires quite high resolution and therefore it was not practical to get information about the mobile vortices from the in-plane resistivity. This is also because the injecting current must be too small to cause heating in such a low- $T_c$  superconductor. However, the out-of-plane resistivity  $\rho_{\perp}$ , which is several orders of magnitude larger than in-plane resistivity in the normal state, is observable with moderate sensitivity. In the vortex state, while the in-plane resistivity comes from the in-plane transport of vortices mentioned above, the out-of-plane resistivity comes from a different mechanism; that is the phase coherency between the layers, so that it is possible to make an experimental study on the out-of-plane dynamical correlation in the vortices. The vanishing of the resistivity signals establishment of the out-of-plane coherence.

As seen in the upper inset of Fig. 12, the out-of-plane resistivity approaches zero with a super-exponential decrease, of which the linear extrapolation to a zero resistivity (the lower inset) gives a characteristic temperature of appearance of the out-of-plane phase coherence. In total five crystals were examined. Thus determined temperatures at several fields for each crystal are plotted in the field-temperature diagram in Fig. 13. The results are all on a single curve without serious sample dependence, supporting that this line characterizes an intrinsic boundary related to an out-of-plane phase coherence. Although the out-of-plane resistive transition is sharp, it has a quite small but nonvanishing tail before vanishing. For the tail part of the resistive transition, how-

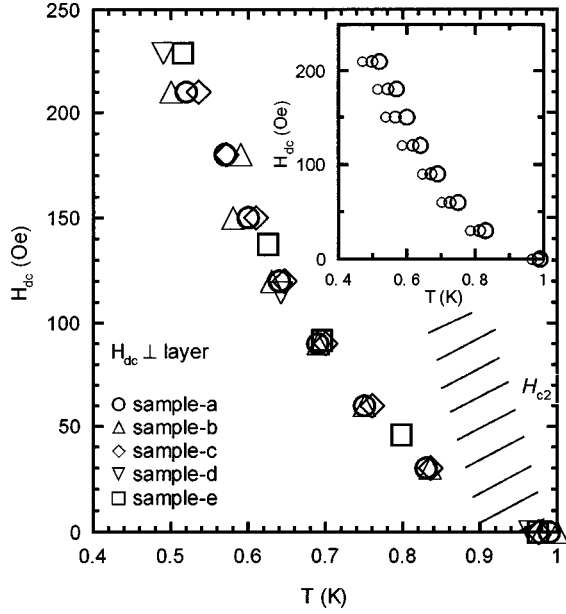


FIG. 13. Offset temperatures of  $\rho_{\perp}$  for five crystals which are distinguished by different symbols. In the inset, open circles with different sizes stand for different definition of the offset temperatures for an identical crystal. For definition, see text.

ever, sample dependence encountered implies that the observation should not be taken as it is. The resistive profiles shown in Fig. 12 are those of a crystal with the smallest resistive tail. Considering the tail part, one can make other definitions of the offset temperatures; for example, the temperature giving  $\rho_n/100$  or  $\rho_n/1000$ , as shown in the inset of Fig. 12, where  $\rho_n$  is the normal-state resistivity at 3 K. Thus defined temperatures are plotted by open circles of the middle and small sizes, respectively, along with the large circles determined by the linear extrapolation in the inset of Fig. 13, where the characteristic temperatures are slightly shifted to the lower temperature side. Such freedom of definition may leave some room for the pursuit of the temperature where the resistivity really vanishes. However, it should be noted that the out-of-plane resistivity comes from the out-of-plane phase fluctuations. In this mechanism, it is reasonable to consider that the out-of-plane resistivity does not perfectly vanish even when the out-of-plane correlation of the pancake vortices are of long range, because thermal excitation of tilting vibrations and out-of-plane phase slippage (vortex rearrangement) may contribute to the finite resistivity in the out-of-plane direction. Thus, we consider that the temperature defined by the linear extrapolation reasonably characterizes the decoupling temperature where the phase coherence is practically established/lost. If the decoupling were the first-order transition, a jump of the out-of-plane resistivity would have been observed. The absence of such an anomaly may suggest that the decoupling is a continuous transition (higher than first order) or a crossover.

### C. $H$ - $T$ phase diagram

The onsets of the out-of-plane  $\chi'$  as the inductive transitions in the low-frequency limit and the offsets of the out-of-plane resistivity are again plotted in Figs. 14(a) and 14(b) along with the  $H_{c2}$  line determined by the specific-heat mea-

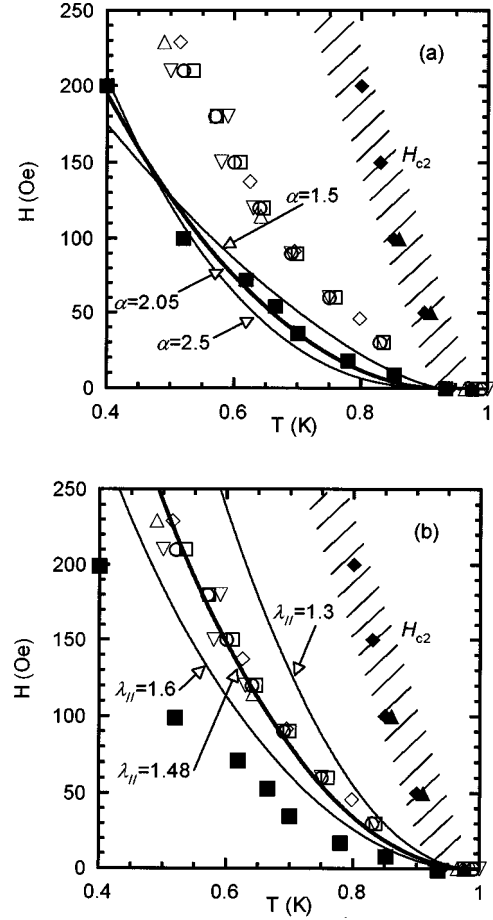


FIG. 14.  $H$ - $T$  phase diagram of ET-NH<sub>4</sub>. The onset temperatures of the inductive transition and the offset ones of the out-of-plane resistive transition are plotted along with the mean-field  $H_{c2}$  line in the  $H$ - $T$  plane and are fitted to the functional forms in the melting theory (a) and the out-of-plane decoupling theory (b), respectively. The bold curves are best fits.

surement under fields. This figure includes two additional data of the out-of-plane  $\chi'$  measured in a dilution refrigerator.<sup>34</sup> In this section, these two kinds of boundaries in the vortex state are discussed in terms of the existing theories.

The  $\chi'$  onsets are fitted to a relation of  $H_m = H_0(1 - T/T_c)^\alpha$ , as predicted by the melting theory with fitting parameters of  $H_0$  and  $\alpha$ . In Fig. 14(a), the thick solid line is the best fit to the data and the obtained values of the parameters are  $H_0 = 592$  G and  $\alpha = 2.05$ . Also shown in the figure are two  $H_m$  curves with exponents of  $\alpha = 1.5$  and  $2.5$  for comparison. The recent melting theory<sup>35</sup> predicts  $\alpha = 2$  for the extremely anisotropic case ( $\gamma s > \lambda_{\parallel}$ ) and  $\alpha = 1.5$  for the moderately anisotropic case ( $\gamma s < \lambda_{\parallel}$ ) in a low-field region. Since ET-NH<sub>4</sub> is an extremely anisotropic case as mentioned before, the fitting value of  $\alpha$  turns out to be in fairly good agreement with the prediction. (It is noted that this theory also explains the experimental value of  $\alpha$  of the melting line for BSCCO observed as the first-order transition in the local magnetic measurement.<sup>2</sup>) The value of  $H_0$  is given in the theory as follows:

$$H_0 = \frac{\Phi^5 c_L^4}{\pi (k_B T_c)^2 \gamma^2 \lambda_{\parallel}(0)^4}. \quad (2)$$

With the fitted value of  $H_0 = 592$  G and  $\lambda_{\parallel}(0)$  of  $0.7 \mu\text{m}$  (see Sec. III B), Eq. (2) gives the Lindemann number  $c_L$  as 0.12. The value of the Lindemann number  $c_L$  is considered to be 0.1–0.2 from the experimental and theoretical investigations of high- $T_c$  oxides (for example, Monte Carlo simulation was performed by Ryu *et al.*<sup>36</sup>). This agreement of  $c_L$  strongly supports that the boundary in question is a melting line.

Next, the offset of the out-of-plane resistivity, defined by the linear extrapolation argued above, is discussed in the context of the 3D-2D vortex decoupling, which is induced by the competition between the out-of-plane coupling of the pancake vortices and the thermal disturbance. By analogy with the Lindemann criterion in the melting, the decoupling of pancake vortices is expected to occur when the root-mean-square interlayer thermal displacement,  $u_T = \langle (u_{n+1} - u_n)^2 \rangle$ , becomes comparable to the intervortex distance  $a_0$ , where  $u_n$  means the position of the pancake vortex in the layer specified by  $n$ . Deamen *et al.*<sup>37</sup> gave a formula for the temperature dependence of the decoupling field  $H_D(T)$  in case of  $\gamma_s > \gamma_{\parallel}$  (extremely anisotropic case) as follows:

$$H_D(T) = \frac{\Phi^3 s}{32\pi^3 T \lambda_{\parallel}(T)^4} \ln \left[ \frac{8\pi^2 T \lambda_{\parallel}(0)^4}{\Phi^2 s^3} \right]. \quad (3)$$

If the relation of  $\lambda_{\parallel}(T) = \lambda_{\parallel}(0) / [1 - (T/T_c)^2]^{1/2}$  is assumed for simplicity, a variable parameter in this formula is only  $\lambda_{\parallel}(0)$ . In Fig. 14(b), a fit to the data is presented. The best fit gives a value of  $\lambda_{\parallel}(0) = 1.48 \mu\text{m}$ . [The curves with  $\lambda_{\parallel}(0) = 1.3$  and  $1.6 \mu\text{m}$  are also shown for comparison.] As seen in the figure, the functional form of Eq. (3) reproduces the experimental data quite well. The fitted value of  $1.48 \mu\text{m}$  is somewhat larger than the value of  $\lambda_{\parallel}(0)$  evaluated as  $0.7 \mu\text{m}$ . It is mentioned that a similar situation was encountered in artificial MoGe/Ge multilayers studied by Steel, White, and Graybeal<sup>38</sup> who discussed the decoupling field in the context of Deamen's theory, although it was a case of the moderately anisotropic superconductor. The decoupling in ET-NH<sub>4</sub> occurs at smaller fields than predicted, while the MoGe/Ge multilayers were reported to show the opposite deviation from the prediction. The difference between the observation and the theory may be suggestive of some room for improvement in the theoretical treatment; for example, incorporation of the neglected ingredients such as the effect of the normal core. Anyway, it is emphasized that the characteristic line, which is explained qualitatively as the decoupling boundary, was found in the mobile vortex region in the  $H$ - $T$  plane.

## VI. CONCLUDING REMARKS

The phenomenological aspect of superconductivity in the quasi-two-dimensional organic conductor,  $\alpha$ -(BEDT-TTF)<sub>2</sub>NH<sub>4</sub>Hg(SCN)<sub>4</sub>, was investigated through the thermodynamic, resistive, and inductive measurements in zero and finite dc fields.

The anisotropy parameter deduced from resistivity and penetration depth amounts to the order of  $10^3$ , which is the largest value among any reported values to date to our

knowledge. Reflecting the large anisotropy and the large in-plane penetration depth, the Ginzburg number of the present superconductor amounts to a quite large value in spite of the low transition temperature, predicting a wide range of the vortex-liquid state. Indeed, a region where the vortices are mobile was observed through both the in-plane and out-of-plane ac susceptibility measurements under fields below the  $H_{c2}$  line, which was determined by the specific-heat measurement.

The large anisotropy also leads the out-of-plane penetration depth to a macroscopic value [ $\lambda_{\perp}(0) = 1.4 \text{ mm}$ ]. In the vortex state, application of a parallel ac field causes the vortex motion in the tilt mode. In this superconductor, a parallel ac field can reach the whole sample volume because  $\lambda_{\perp}$  is comparable to or larger than the sample size. This feature permits the whole vortices to be driven directly by the parallel ac field, not via the diffusion process. Using this profit in the investigation of the vortex dynamics, we found the characteristic line which indicates the drastic change of mobility of the vortices. With the observation of absence of frequency dependence we conclude that this is a melting line of vortex lattice or glass, not a crossover of vortex dynamics.

The out-of-plane resistivity under perpendicular fields gave the sample-independent characteristic line in the mobile vortex phase in the  $H$ - $T$  plane, which is suggestive of the interlayer coupling/decoupling of the melted pancake vortices.

The superconducting parameters obtained in the present study show that the pancake vortices in  $\alpha$ -(BEDT-TTF)<sub>2</sub>NH<sub>4</sub>Hg(SCN)<sub>4</sub> are mainly coupled through the electromagnetic energy. Reflecting this, the temperature dependence of the two lines determined by inductive and out-of-plane resistive transitions under fields was consistent with the recent melting theory and the decoupling theory taking account of the electromagnetic coupling.

In the quasi-two-dimensional vortex system, the morphology of the pancake vortices is now an open question. There are several possible phases of the vortex matter; the unconnected pancake-vortex gas, line liquid and solids such as lattice, glass, and semiglass. One of the experiments performed for BSCCO suggested the occurrence of the sublimation transition<sup>39</sup> at a line which separates the solid phase from the gas phase in the  $H$ - $T$  plane, although there still exists controversy.<sup>12,35</sup> The present system does not follow the sublimation transition but suggests a two-step transition consisting of melting and evaporation. This fact may suggest that the pancake vortex system mainly coupled through the electromagnetic energy has a different route to solidification of vortices from that in BSCCO where Josephson energy dominates the coupling of the pancake vortices. However, the following aspects may also be involved in the separation of the melting and evaporation in the present system. One is the huge coherence length of ET-NH<sub>4</sub>, which is one order of magnitude larger than that of BSCCO, as mentioned above. The large vortex core strongly affects the pinning and the out-of-plane coupling of the pancake vortices. Another is morphology of defects which pin the vortices. Experiments with samples where the type of defect is controlled will be helpful to elucidate this.

## ACKNOWLEDGMENTS

We thank K. Kato and T. Takayama in the Low-Temperature Center at IMS for their technical support in low-temperature experiments. This work was supported in

part by Grant-in-Aid for Scientific Research Nos. 06243102 (Priority Area ‘‘Novel Electronic States in Molecular Conductors’’) and 06452064 from the Ministry of Education, Science, Sports, and Culture, Japan.

- <sup>1</sup>H. Safar, P. L. Gammel, D. A. Huse, and D. J. Bishop, *Phys. Rev. Lett.* **69**, 824 (1992).
- <sup>2</sup>E. Zeldov, D. Mayer, M. Konczykowski, V. B. Geshkenbein, V. M. Vinokur, and H. Shtrikman, *Nature (London)* **375**, 373 (1995).
- <sup>3</sup>A. Shilling, R. A. Fisher, N. E. Phillips, U. Welp, D. Dasgupta, W. K. Kwok, and G. W. Crabtree, *Nature (London)* **382**, 791 (1996).
- <sup>4</sup>For a review, see G. Blatter, M. V. Feigel'man, V. B. Geshkenbein, A. I. Larkin, and V. M. Vinokur, *Rev. Mod. Phys.* **66**, 1125 (1994).
- <sup>5</sup>W. E. Lawrence and S. Doniach, in *Proceedings of the Twelfth International Conference on Low-Temperature Physics, Kyoto 1970*, edited by E. Kanda (Keigaku, Tokyo, 1970), p. 361.
- <sup>6</sup>L. I. Glazman and A. E. Koshelev, *Phys. Rev. B* **43**, 2835 (1991).
- <sup>7</sup>M. V. Feigel'man, V. B. Geshkenbein, and A. I. Larkin, *Physica C* **167**, 177 (1990).
- <sup>8</sup>R. Ikeda, *J. Phys. Soc. Jpn.* **64**, 1693 (1995).
- <sup>9</sup>T. Tamegai, Y. Iye, I. Oguro, and K. Kishio, *Physica C* **213**, 33 (1993).
- <sup>10</sup>R. Cubitt, E. M. Forgan, G. Yang, S. L. Lee, D. M. Paul, H. A. Mook, M. Yethiraj, P. H. Kes, T. W. Li, A. A. Menovsky, Z. Tarnawski, and K. Mortensen, *Nature (London)* **365**, 407 (1993).
- <sup>11</sup>S. L. Lee, M. Warden, H. Keller, J. W. Schneider, D. Zech, P. Zimmermann, R. Cubitt, E. M. Forgan, M. T. Wylie, P. H. Kes, T. W. Li, A. A. Menovsky, and Z. Tarnawski, *Phys. Rev. Lett.* **75**, 922 (1995).
- <sup>12</sup>R. A. Doyle, D. Liney, W. S. Seow, and A. M. Campbell, *Phys. Rev. Lett.* **75**, 4520 (1995).
- <sup>13</sup>B. Khaykovich, E. Zeldov, D. Majer, T. W. Li, P. H. Kes, and M. Konczykowski, *Phys. Rev. B* **76**, 2555 (1996).
- <sup>14</sup>M. Lang, F. Steglich, N. Toyota, and T. Sasaki, *Phys. Rev. B* **49**, 15 227 (1994).
- <sup>15</sup>T. Takahashi, T. Tokiwa, K. Kanoda, H. Urayama, H. Yamochi, and G. Saito, *Physica C* **153-155**, 487 (1988); *Synth. Met.* **27**, A319 (1988); K. Kanoda, K. Sakao, T. Takahashi, T. Komatsu, and G. Saito, *Physica C* **185-189**, 2667 (1991); T. Takahashi, K. Kanoda, and G. Saito, *ibid.* **185-189**, 366 (1991); S. M. De Soto, C. P. Slichter, H. H. Wang, U. Geiser, and J. M. Williams, *Phys. Rev. Lett.* **70**, 2956 (1993); H. Mayaffre, P. Wzietek, D. Jerome, and S. Brazovskii, *ibid.* **76**, 4951 (1996).
- <sup>16</sup>M. Oshima, H. Mori, G. Saito, and K. Oshima, *Chem. Lett.* **1989**, 1159.
- <sup>17</sup>H. H. Wang, K. D. Carlson, U. Geiser, W. K. Kwok, M. D. Vashon, J. E. Thompson, N. F. Larsen, G. D. McCabe, R. S. Hulscher, and J. M. Williams, *Physica C* **166**, 57 (1990).
- <sup>18</sup>J. S. Brooks, X. Chen, S. J. Klepper, S. Valfells, G. J. Athas, Y. Tanaka, T. Kinoshita, N. Kinoshita, M. Tokumoto, H. Anzai, and C. C. Agosta, *Phys. Rev. B* **52**, 14 457 (1995).
- <sup>19</sup>H. Taniguchi, H. Sato, Y. Nakazawa, and K. Kanoda, *Phys. Rev. B* **53**, R8879 (1996); H. Sato, H. Taniguchi, Y. Nakazawa, A. Kawamoto, K. Kato, and K. Kanoda, *Synth. Met.* **70**, 915 (1995).
- <sup>20</sup>R. Bush, G. Ries, H. Werthner, G. Kreiselmeyer, and G. Saemann-Ischenko, *Phys. Rev. Lett.* **69**, 522 (1992).
- <sup>21</sup>S. Martin, A. T. Fiory, R. M. Fleming, L. F. Schneemeyer, and J. V. Waszczak, *Phys. Rev. Lett.* **60**, 2194 (1988).
- <sup>22</sup>K. Murata, M. Tokumoto, H. Anzai, Y. Honda, N. Kinoshita, T. Ishiguro, N. Toyota, T. Sasaki, and Y. Muto, *Synth. Met.* **27**, A263 (1988).
- <sup>23</sup>L. P. Le, G. M. Luke, B. J. Sternlieb, W. D. Wu, Y. J. Uemura, J. H. Brewer, T. M. Riseman, C. E. Stronach, G. Saito, H. Yamochi, H. H. Wang, A. M. Kini, K. D. Carlson, and J. M. Williams, *Phys. Rev. Lett.* **68**, 1923 (1992); D. R. Harshman, A. T. Fiory, R. C. Haddon, M. L. Kaplan, T. Pfiz, E. Koster, I. Shinkoda, and D. L. Williams, *Phys. Rev. B* **49**, 12 990 (1994).
- <sup>24</sup>M. Lang, N. Toyota, T. Sasaki, and H. Sato, *Phys. Rev. Lett.* **69**, 1443 (1992).
- <sup>25</sup>For example, T. Sasaki, H. Sato, and N. Toyota, *Solid State Commun.* **76**, 507 (1990).
- <sup>26</sup>As the value of  $m_{\alpha}^*$ , we averaged the two reported values of the SdH mass;  $2.1m_0$  [T. Osada, A. Kawasumi, R. Yagi, S. Kagoshima, N. Miura, H. Mori, T. Nakamura, and G. Saito, *Solid State Commun.* **75**, 901 (1990)],  $2.5m_0$  [S. Uji, T. Terashima, H. Aoki, J. S. Brooks, M. Tokumoto, N. Kinoshita, T. Kinoshita, Y. Tanaka, and H. Anzai, *Phys. Rev. B* **54**, 9332 (1996)]. The dHvA mass has a similar value [J. Wosnitza, G. W. Crabtree, H. H. Wang, K. D. Carlson, M. D. Vashon, and J. M. Williams, *Phys. Rev. Lett.* **67**, 263 (1991)].
- <sup>27</sup>K. Oshima, T. Mori, H. Inokuchi, H. Urayama, H. Yamochi, and G. Saito, *Phys. Rev. A* **38**, 938 (1988).
- <sup>28</sup>G. Deutscher and O. E. Wohlman, *J. Phys. C* **10**, L433 (1977).
- <sup>29</sup>A. Carrington, A. P. Mackenzie, and A. Tyler, *Phys. Rev. B* **54**, R3788 (1996).
- <sup>30</sup>B. Andraka, G. R. Stewart, K. D. Carlson, H. H. Wang, M. D. Vashon, and J. M. Williams, *Phys. Rev. B* **42**, 9963 (1990).
- <sup>31</sup>For  $\xi_{\parallel}$  (or  $H_{c2\parallel}$ ), J. E. Graebner, R. C. Haddon, S. V. Chichester, and S. H. Glarum, *Phys. Rev. B* **41**, 4808 (1990), for  $\lambda_{\parallel}$ , Refs. 23 and 24 and for  $\lambda_{\perp}$ , K. Kanoda, Y. Tsubokura, K. Ikeda, T. Takahashi, N. Matsukawa, G. Saito, H. Mori, B. Hilti, and J. S. Zambounis, *Synth. Met.* **55-57**, 2865 (1993) and P. A. Mansky, P. M. Chaikin, and R. C. Haddon, *Phys. Rev. B* **50**, 15 929 (1994).
- <sup>32</sup>For  $\xi_{\parallel}$  (or  $H_{c2\parallel}$ ), A. S. Alexandorov, V. N. Zavaritsky, W. Y. Liang, and P. L. Nevsky, *Phys. Rev. Lett.* **76**, 983 (1996), for  $\lambda_{\parallel}$ , D. R. Harshman, R. N. Kleiman, M. Inui, G. P. Espinosa, D. B. Mitzi, A. Kapitulnik, T. Pfiz, and D. L. Williams, *ibid.* **67**, 3152 (1991) and T. Shibauchi, A. Maeda, H. Kitano, T. Honda, and K. Uchinokura, *Physica C* **203**, 315 (1992) and for  $\lambda_{\perp}$ , T. Jacobs, S. Sridhar, Qiang Li, G. D. Gu, and N. Koshizuka, *Phys. Rev. Lett.* **75**, 4516 (1995).
- <sup>33</sup>A. E. Koshelev, *Phys. Rev. Lett.* **76**, 1340 (1996).

- <sup>34</sup>Y. Nakazawa, H. Sato, A. Kawamoto, K. Kato, and K. Kanoda, *Synth. Met.* **70**, 919 (1995).
- <sup>35</sup>G. Blatter, V. Geshkenbein, A. Larkin, and H. Nordborg, *Phys. Rev. B* **54**, 72 (1996).
- <sup>36</sup>S. Ryu, S. Doniach, G. Deutscher, and A. Kapitulnik, *Phys. Rev. Lett.* **68**, 710 (1992).
- <sup>37</sup>L. L. Deamen, L. N. Bulaevskii, M. P. Maley, and J. Y. Coulter, *Phys. Rev. Lett.* **70**, 1167 (1993); *Phys. Rev. B* **47**, 11 291 (1993).
- <sup>38</sup>D. G. Steel, W. R. White, and J. M. Graybeal, *Phys. Rev. Lett.* **71**, 161 (1993).
- <sup>39</sup>D. G. Fuchs, R. A. Doyle, E. Zeldov, D. Majer, W. S. Seow, R. J. Drost, T. Tamegai, S. Ooi, M. Konczykowski, and P. H. Kes, *Phys. Rev. B* **55**, R6156 (1997).